JOURNAL OF GEOPHYSICAL RESEARCH, VOL. 105, NO. A8, PAGES 18,639–18,653, AUGUST 1, 2000

The cross-polar potential drop and its correlation to the solar wind

S. Eriksson

Alfvén Laboratory, Royal Institute of Technology, Stockholm, Sweden

R. E. Ergun[1] and C. W. Carlson

Space Sciences Laboratory, University of California, Berkeley

W. Peria

Department of Geophysics, University of Washington, Seattle

Abstract. The cross-polar potential drop Φ_{pc} as derived from the FAST satellite is used to study the average magnetospheric response to changes in the solar wind as monitored by the Wind spacecraft. The coupling of the solar wind with the magnetosphere is examined using the interplanetary magnetic field (IMF) B_z, the model reconnection electric field $vB_t\sin^k(\theta/2)$ for k=3, 4, and the Akasofu-Perreault ϵ parameter. Initial results comprising 37 cases of Φ_{pc} show one major response of the magnetosphere to the solar wind forcing at 15 min time lag followed by two minor pulses at 55 min and 105 min, respectively, during times when the IMF polarity was mainly southward and the geomagnetic activity was moderate to low. Φ_{pc} shows a very good correlation with typical models of the reconnection electric field at 15 min time lag, reaching a maximum linear correlation coefficient of r=0.95 for $vB_t\sin^3(\theta/2)$. In order to reach an understanding of the importance of individually calculated correlation coefficients, we introduce the statistical bootstrap algorithm of *Efron and Tibshirani* [1993], which allows us to estimate a correlation coefficient standard error. In defining a quality measure based on this method, the significance coefficient s, we are able to interpret a resulting correlation coefficient time lag series in terms of a linear prediction filter similar to earlier techniques. The results on the magnetospheric response for Φ_{pc} are further compared with those obtained using the geomagnetic indices *Dst*, *SYM-H*, and *ASY-H*. The similar magnetospheric response to the solar wind electric field for Φ_{pc} and *ASY-H* at time delays of more than 40 min together with a high correlation coefficient between Φ_{pc} and *ASY-H* suggest that these magnetospheric parameters couple to one another. The average dynamic response of the ionospheric convection to the solar wind electric field is in essential agreement with those reported by *Klimas et al.* [1994] on a normal magnetospheric mode with a recurrence frequency of 50 min.

1. Introduction

There exist two phenomenological models for the description of the temporal magnetospheric response to the continuous forcing of the solar wind [*Rostoker et al.*, 1987]. These are the directly driven model [*Perreault and Akasofu*, 1978; *Akasofu*, 1980] and the loading-unloading model [*McPherron et al.*, 1973; *Baker et al.*, 1979; *Hones*, 1979]. The driven model is characterized by a time lag between the solar wind energy input in some magnetopause energy-coupling region and dissipation into the ionosphere which depends on the convection time of transferred energy. The unloading model involves the storage of magnetic energy in the current systems of the magnetotail until it reaches a level of critical flux [*Klimas et al.*, 1992] whereupon a fraction of the stored total energy is released impulsively at substorm expansion onset. The time lag for the loading-unloading process will thus be dependent on the timescales controlling substorms.

Bargatze et al. [1985] correlated the rectified solar wind electric field vB_s (B_s being the southward compo-

[1]Now at the Department of Astrophysical and Planetary Science, Laboratory for Atmospheric and Space Physics, University of Colorado, Boulder.

Copyright 2000 by the American Geophysical Union.

Paper number 2000JA900033.
0148-0227/00/2000JA900033$09.00

nent of the IMF) to the *AL* index and found a bimodal filter shape with one peak near 20-min time lag and a second peak near 60-min delay. The amplitudes of these peaks were shown to vary with the level of geomagnetic activity, where the amplitude of the first peak dominates for strongly active periods. They conclude that the near 20-min delay corresponds to the onset of the growth phase and *DP* 2 convection, while the second delay corresponds to the *DP* 1 convection of the substorm current wedge. It is interesting to note here that they did not report more than two peaks using their linear prediction filter.

Farrugia et al. [1993] in their study of a magnetic cloud event identified 23 individual substorm onsets during a 20-hour period when the interplanetary magnetic field (IMF) was southward. The shortest interval between two substorms was found to be ~25 min and the longest was ~100 min, while on the average substorms recurred once every ~50 min. They further concluded that the recurrence frequency appeared to be insensitive to the strength of the interplanetary energy input as measured by vB_s and the Akasofu-Perreault ϵ parameter [*Perreault and Akasofu,* 1978; *Akasofu,* 1980], where $\epsilon = vB^2\sin^4(\theta/2)l_0^2$, v is the solar wind speed, B is the IMF magnitude, θ is the IMF clock angle, and the constant $l_0 \sim 7R_E$ denotes the linear dimension of the cross section of the solar wind-magnetosphere coupling region.

Klimas et al. [1994] constructed a Faraday loop model which is shown to predict the 50-min average unloading rate of *Farrugia et al.* [1993] as well as the near 60-min peak of the *Bargatze et al.* [1985] bimodal filter. Both responses were interpreted in terms of an unloading normal mode of the magnetosphere. They further concluded that this mode is best demonstrated through linear prediction filter analyses such as the construction of *Bargatze et al.* [1985]. Judging by the results of *Farrugia et al.* [1993] and *Klimas et al.* [1994], the substorm process is closely related to the unloading mechanism of the magnetotail.

There is some further debate on what role substorms play regarding the physical processes involved in the main phase injection of ring current particles [*Chen et al.,* 1994]. *Lyons and Williams* [1980] proposed that global convection is one basis of ring current injection rather than the expansion phase of substorms. The idea of an enhanced global convection electric field was also suggested by *Clauer and McPherron* [1980] as a direct cause for the partial ring current development. It was later proposed that a fluctuating global convection electric field may be a cause of magnetic storms [*McPherron,* 1997]. These fluctuations may have different sources, such as magnetospheric waves or substorm expansions, and appear to be essential for the moving of particles from open to closed drift paths in a manner resembling radial diffusion [*Lyons and Schulz,* 1989].

Based on the ideas put forth in the papers mentioned above, both regarding the importance of a fluctuating global convection electric field for ring current injection and the proposed existence of a normal unloading recurrence mode in the dynamics of the magnetosphere, we choose to study the magnetospheric response to the solar wind input by using the cross-polar potential drop Φ_{pc} rather than the *Dst* or *AL* index time series usually adopted in linear prediction filters. The approach described below is to perform a statistical linear correlation study between 5-min averaged solar wind parameters measured by the Wind spacecraft and a discrete series of 37 cross-polar potential drop measurements by the FAST satellite in a corotating frame of reference.

Our aim is to show that the average response of the dynamical magnetosphere to the solar wind energy input can be studied by the global convection electric field as measured by polar orbiting satellites, despite the lack of a continuous time series coverage of Φ_{pc} measurements. This is mainly achieved by applying the statistical bootstrap algorithm [*Efron and Tibshirani,* 1993] on a time series of linear correlation coefficients between the solar wind and the magnetospheric parameters. The bootstrap algorithm provides us with an estimate of the correlation coefficient standard error which is included in our definition of a significance coefficient s. This parameter may be described as an objectively weighted or filtered correlation coefficient.

The electric potential difference across the polar cap is a fundamental measure of the coupling between the solar wind and the Earth's magnetosphere [e.g., *Harel et al.,* 1981; *Wolf et al.,* 1982]. Several functional forms have been demonstrated in the literature on both empirical and theoretical grounds as reasonable approximations for the dependence of Φ_{pc} on various interplanetary physical quantities such as the magnitude of the IMF and the solar wind speed v [*Wygant et al.,* 1983; *Reiff and Luhmann,* 1986; *Gonzalez et al.,* 1994, and references therein].

An empirical form of the reconnection electric field which correlates well with Φ_{pc} is $vB_t\sin^k(\theta/2)$, where v is the solar wind speed, $B_t = (B_y^2 + B_z^2)^{\frac{1}{2}}$ is the projection of the IMF onto the GSM y-z plane, and $\theta = \tan^{-1}(B_y/B_z)$ is the clock angle between B_t and the geomagnetic field vector projected at the magnetopause. The angular dependence is empirically controlled by k, usually taken to be k=2, 3, or 4. *Reiff and Luhmann* [1986] reported on a high correlation for k=3, and *Wygant et al.* [1983], when using k=4, refer to an intermediate model between the *Kan and Lee* [1979] model and the half wave rectifier model of *Burton et al.* [1975] with the same angular dependence as the ϵ parameter.

In the present paper, we shall consider the solar wind-magnetosphere coupling quantities IMF B_z, the reconnection electric field $vB_t\sin^k(\theta/2)$ for k=3 and k=4 (hereby referred to as Erec3 and Erec4), and the ϵ parameter, respectively, to be correlated with Φ_{pc}. The IMF data are expressed in geocentric solar magnetic (GSM) coordinates.

2. Data

The FAST satellite was launched from the Western Test Range at Vandenberg Air Force Base on August 21, 1996, by a Pegasus-XL vehicle that placed FAST into an 83° inclination elliptical orbit of 350 km by 4175 km altitude [*Carlson et al.*, 1998]. The satellite is spin stabilized with a spin period of 5 s, oriented in a "cartwheel" attitude having the spin axis nearly (negative) normal to the orbital plane. The in situ electric field is measured with a three-axis dipole antennae with 56, 8, and 5 m baselines. Although one of the wire booms in the spin plane did not deploy properly, the remaining three booms are sufficient to measure vector electric fields (R. E. Ergun, personal communication, 1998).

The electric potential along the path of the FAST satellite is obtained by integrating the electric field $\mathbf{E}$ in the direction of the satellite velocity $\mathbf{v}$. The measured electric field $\mathbf{E}' = \mathbf{E} + \mathbf{v} \times \mathbf{B}$ is known along two perpendicular vectors in the spin plane and the unknown spin axis electric field is assumed zero. Since we are interested in the electric field component along the direction of motion and the spin axis is nearly normal to the orbital plane, the contribution of an electric field along the spin axis is assumed negligible.

In this study, all polar cap passes begin and end at invariant latitudes less than approximately 63 degrees and the actual integration is performed by setting the potential to zero at the beginning of each satellite pass. In an ideal situation the potential should thus return to zero at subauroral latitudes after each completed polar pass, since the corotating plasmasphere will stay at approximately constant potential in a corotating frame of reference. However, this is usually not the case. There are several reasons why a mismatch occurs. Inexact knowledge of the satellite's attitude and the use of a model geomagnetic field may cause errors in the calculation of $\mathbf{v} \times \mathbf{B}$ which will affect the electric field $\mathbf{E}$ and thus the calculation of the potential. An incomplete total electric field due to a missing third, axial component may also affect the resulting electric potential by an accumulation of a small term. Following *Shue and Weimer* [1994], we correct for these electric field offsets by adding a constant electric field to the original data to force a match between the low-latitude potentials on opposite sides of the polar cap. This correction term is found to be of the order of 1 to 2 mV/m with an average correction field of 0.86 mV/m and a maximum correction of 2.72 mV/m.

In order to measure as much of the total cross-polar potential as possible, we look primarily for those dawn to dusk passes that approximately cut across the potential extrema of an imagined *Heppner and Maynard* [1987] statistical two-cell convection pattern with a dawn potential maximum located between 5 and 6 magnetic local time (MLT) and a dusk potential minimum located between 17 and 18 MLT. The preference of a clear two-cell convection pattern for Φ_{pc} introduces a bias in the IMF data toward southward components as is implied by dayside reconnection driven convection.

Several sets of data are used in this statistical study that covers the period from July 7, 1997, until July 24, 1997. The two main sets comprise (1) a discrete series of Φ_{pc} from 37 FAST passes in the Northern Hemisphere, distributed in an invariant latitude and magnetic local time sector as shown in Figure 1, and (2) a continuous series of averaged solar wind plasma and IMF measurements at 5-min time resolution from the Wind spacecraft.

Baker [1986] notes that geomagnetic storm timescales are in the many hours to daily range, while substorm timescales on the other hand are in the several minutes resolution range. Since we will study the general temporal response of the magnetosphere under continuous solar wind forcing and the statistical relationship between the global convection electric field and substorm recurrences, we are primarily interested in studying physical processes on the 5-min timescale.

An additional set of data consisting of three geomagnetic disturbance indices is provided by the World Data Center C for Geomagnetism in Kyoto, Japan. The applied indices are the *Dst*, *SYM-H*, and *ASY-H*, respectively. This set is correlated to the identical set of solar wind data and in the same manner as Φ_{pc} in order to study the corresponding average geomagnetic response for the same conditions.

The *Dst* index has been used extensively as an indicator of storm time onsets [*Gonzalez et al.*, 1994, and references therein] and is included here in spite of its coarse hourly temporal resolution for comparison with earlier linear prediction filter results of the magnetospheric response [e.g., *Clauer et al.*, 1983; *Bargatze et al.*, 1985]. Since the measured Φ_{pc} basically is an integrated time average over a 10-20 min time period (the elapsed time between the satellite measurements of Φ_+ and Φ_-), we select each corresponding *Dst* value from the hour being as close as possible to this interval in order to cover the same period as Φ_{pc}.

The 1-min resolution *SYM-H* index (symmetric disturbance field in horizontal direction) is essentially a high-time resolution *Dst* index [*Iyemori and Rao*, 1996] and is averaged over the same period as the individual cross-polar potential. Following *Iyemori and Rao* [1996] who study the relationship between the ring current development and substorm onsets using both symmetric and asymmetric disturbance indices, we include the asymmetric 1-min resolution *ASY-H* index [*Iyemori and Rao*, 1996], which indicates magnetic disturbances in the horizontal direction on the ground from various current systems such as the partial ring current, field-aligned currents and the substorm current wedge. This index is basically the same as the *ASYM* index used by *Clauer et al.* [1983] and corresponds in a general sense to the *DP* 1 and *DP* 2 current systems. Both the *SYM-H* and the *ASY-H* indices are derived using six stations, a majority of which are at higher latitudes

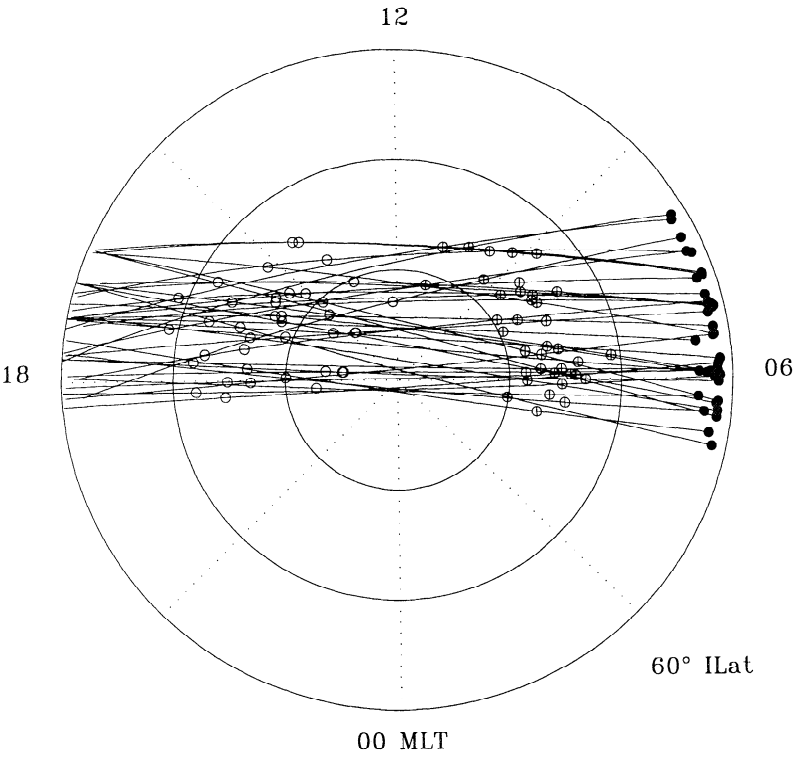

Figure 1. Invariant latitude and magnetic local time coverage of all 37 FAST orbits. The solid circles mark the start point of all dawn-dusk polar passes, while the open circles mark the location of each dawn and dusk cell encountered along the orbit. The orbits cover the period from July 7, 1997, until July 24, 1997.

than the four stations used in the derivation of the *Dst* index.

3. Statistical Analysis and Observations

The correlations between Φ_{pc} and each of the corresponding averaged geomagnetic indices are illustrated in Figure 2 along with the correlation between the *SYM-H* and the *Dst* index, which shows their reported essential agreement. It is interesting to note that a maximum correlation coefficient of r=0.81 is found between Φ_{pc} and *ASY-H*, which implies a coupling between the two parameters.

3.1. Method of Solar Wind Propagation

Is Wind a useful predicting instrument for our attempted correlation analyses between the solar wind input and the magnetospheric response? In the summary of *King* [1986] on the effectiveness of ISEE 3 (200-260 R_E upstream position in 1978-1982) as a monitor of IMF conditions, they report that there is some evidence of degradation as ISEE 3 moves away from the Earth-Sun line. No difference was discovered though in the ability of ISEE 3 to predict plasma parameter values as long as the spacecraft was within 50 R_E from this plane. It is therefore concluded that Wind is a favorable monitor of the solar wind conditions in July 1997, since the spacecraft is within 45 R_E from the Earth-Sun line and closer than 90 R_E in its upstream X_{GSE} position.

As a consequence of the spatial separation between Wind and the magnetopause coupling region, it is necessary to obtain an approximate time delay, the propagation time t_p, allowing for a corresponding solar wind transient to reach an assumed average magnetopause location of 11 R_E from the Earth [*Fairfield*, 1971]. The following solar wind propagation delay model assumes that (1) upstream plasma conditions are spatially uniform over a few tens of R_E, (2) solar wind transients are parallel to phase fronts in the GSE x-y plane, and (3) no further delays are introduced by the bow shock. The last assumption leads to an underestimate of the propagation time since the plasma bulk speed is lower in the magnetosheath. This may be corrected for by adding an extra time delay to the final results as we do in our discussion. The front normal at Wind is assumed parallel to the solar wind x-y velocity averaged over 1 hour prior to the time when FAST encounters the dawn cell maximum potential. The time of propagation for each front is then computed by assuming a distance of closest approach in the direction of its normal to a magnetopause coupling region at 11 R_E.

The global magnetosphere convection changes at some unknown rate as FAST moves across the polar cap region. The resulting cross-polar potential difference in-

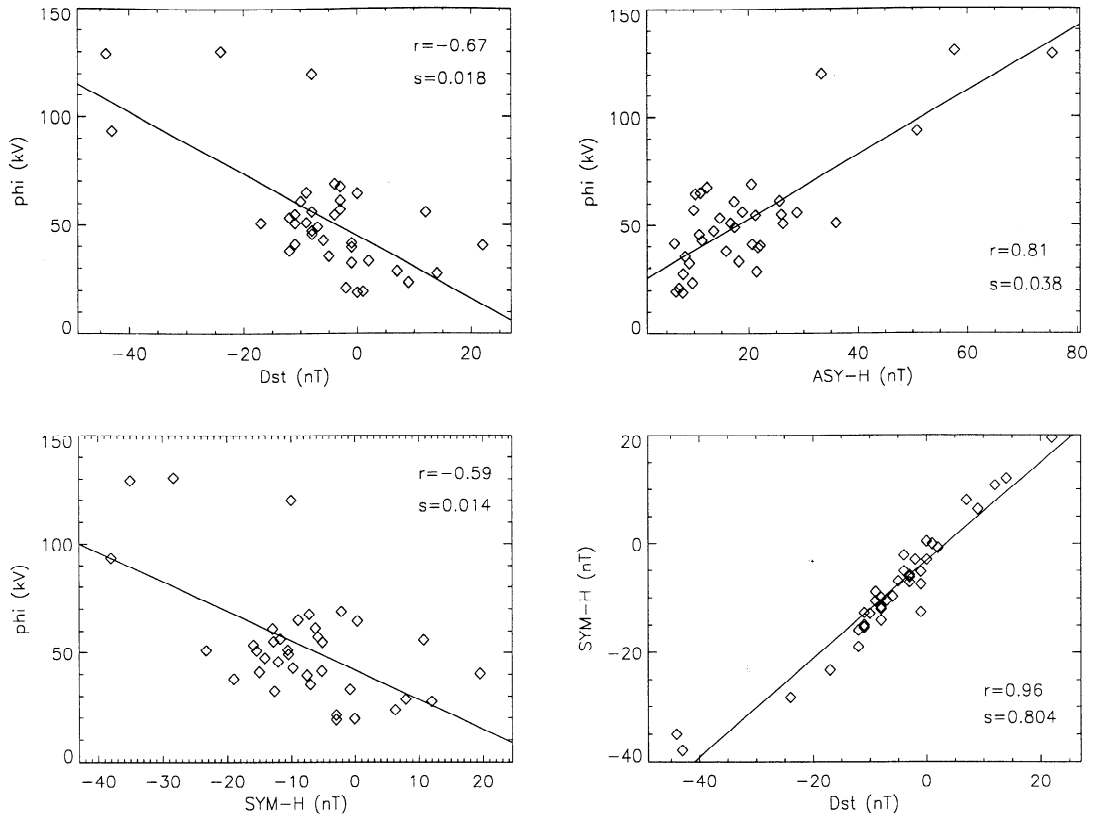

Figure 2. (top, and bottom left) The correlations between Φ_{pc} and the three geomagnetic indices *Dst*, *SYM-H*, and *ASY-H*. Both *SYM-H* and *ASY-H* are averaged over the time between Φ_+ and Φ_-, whereas the *Dst* is the closest hourly average to this interval. (bottom right) The correlation between *SYM-H* and *Dst*. The correlation coefficient r and significance coefficient s (see text) are also indicated.

tegrated between a maximum potential at time t_1 and a minimum potential at time t_2 may therefore be understood as a time average and not as an instantaneous measure of the prevailing state of the global magnetospheric convection. In order to correlate a set of 37 cross-polar potential drops with a corresponding set of a specific interplanetary parameter, we find the individual times of correlation by the following procedure. First locate t_m, the time midway between t_1 and t_2, since we treat the calculated Φ_{pc} as a time-averaged quantity. Then subtract the individually estimated propagation times from t_m for each case. The resulting time t_0 is the initial reference time for which the solar wind has reached an assumed average magnetopause location of 11 R_E and the center of the 5-min time averaging interval at zero time lag for which all four solar wind parameters are averaged.

By moving the time averaging window in steps of 5 min back in time from t_0, that is, toward positive time lag, we examine how the transferred solar wind energy convects in the magnetospheric system. For each new set of 37 correspondingly averaged solar wind parameters, we calculate a new correlation coefficient with Φ_{pc} in order to find the time lag where the correlation coefficient maximizes. We further avoid any precondition on causality between the solar wind input and the magnetospheric output as measured by Φ_{pc} and the geomagnetic indices by moving the averaging window forward in time from t_0 as well, that is, in the direction of negative time lag.

How far we can move in either direction using this correlation coefficient technique turns out to be limited by the sampling period of the FAST satellite or rather the minimum separation between any two consecutive t_0 which is about 130 min. The IMF consists of a broad spectrum of frequencies and a resonance will occur in the final time lag series of the correlation coefficient at an IMF frequency corresponding to the minimum sampling period. This is apparent in the 5-min resolution time series of the linear correlation coefficient between Φ_{pc} and the four solar wind parameters IMF B_z, Erec4, Erec3, and ϵ (see Figure 3) where the center of the final averaging window is displaced 20 hours in both directions from each of the 37 t_0. We notice that the correlation coefficient oscillates symmetrically on both sides of the time lag where a maximum correlation is found. A fast Fourier transform on each of the four time series results in an approximate period of 135 min for the oscillation, which at this resolution practically coincides with the minimum consecutive time period. We will

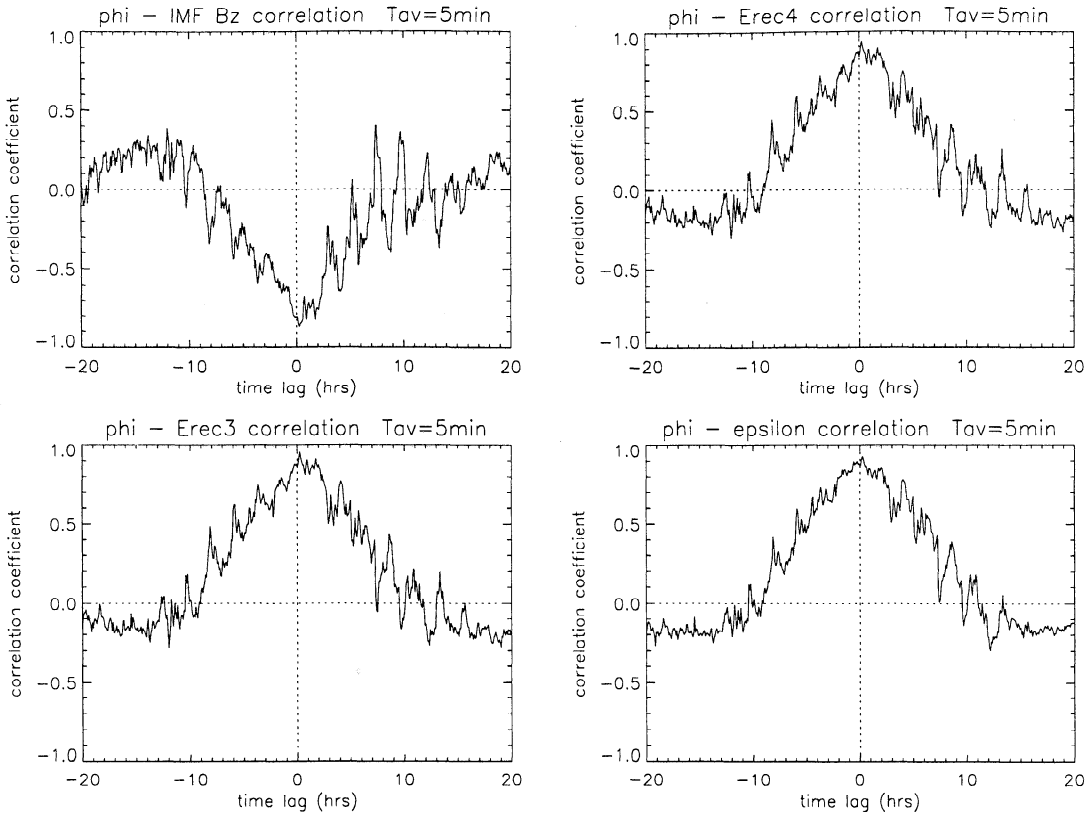

Figure 3. The time lag evolution of 5-min resolution correlation coefficients between Φ_{pc} and four solar wind parameters as indicated above each plot for a total period of ± 20 hours.

thus limit our study of the magnetospheric response to the solar wind input to a time lag window starting at $t_0 - 120$ min and ending at $t_0 + 180$ min.

3.2. Correlation Coefficient Analysis

By replacing Φ_{pc} with *ASY-H* we perform the same correlation with the identical set of solar wind parameters and retrieve the correlation coefficient time series for *ASY-H* as well. In Figure 4a we have plotted the two correlation coefficient time series for Φ_{pc} and *ASY-H* corresponding to the same solar wind parameter as shown at the top in each of four plots. The maximum correlation coefficient and the time lag Δt where this occurs are indicated for each of the time series. The correlation coefficient between Φ_{pc} and the solar wind is maximized at 15-min time lag for all four solar wind parameters, whereas the maximum correlation coefficient for *ASY-H* is reached either at 75-min time lag for IMF B_z and ϵ, or at 60-min time lag for Erec4 and Erec3. An overall maximum correlation coefficient of r=0.95 is obtained between Φ_{pc} and Erec3, whereas the maximum correlation coefficient for *ASY-H*, r=0.90, is reached with ϵ. We further note two interesting details which are most apparent for the two models of the reconnection electric field. First of all, the direct response in Φ_{pc} during the first 40 min is not present in the correlation time series for *ASY-H*. Second, we note how the correlation coefficient for both Φ_{pc} and *ASY-H* closely follow each other between approximately 40-min and 140-min time lag.

In Figure 4b we have replaced Φ_{pc} by *Dst* and *SYM-H* and performed the corresponding correlation for these geomagnetic disturbance indices to the solar wind forcing. Here the maximum correlation coefficient is reached at 70-min time lag for both *Dst* and *SYM-H* independent of solar wind parameter. We observe further how the correlation coefficient time series follow each other at all time lags as is expected from the essential agreement between the two indices (see Figure 2). However, it is clear that the hourly averaged *Dst* index at all time lags is better correlated to the solar wind input than the *SYM-H* index which is averaged over the same time interval as the cross-polar potential drop.

How reliable are these correlation coefficients? How good is, for example, r=0.80 in comparison with r=0.70 or r=0.90? As an example, *Boyle et al.* [1997] apply the reduced chi-square parameter along with the correlation coefficient in their correlative study of Defense Meteorological Satellite Program and hourly averaged IMP 8 data for the derivation of empirical models of Φ_{pc}. By studying their Figure 2, we observe that there is a nearly inverse relationship between these two parameters. If the correlation in some meaning is high, then the reduced chi-square in general is low. Either measure thus provides the same qualitative outcome. We

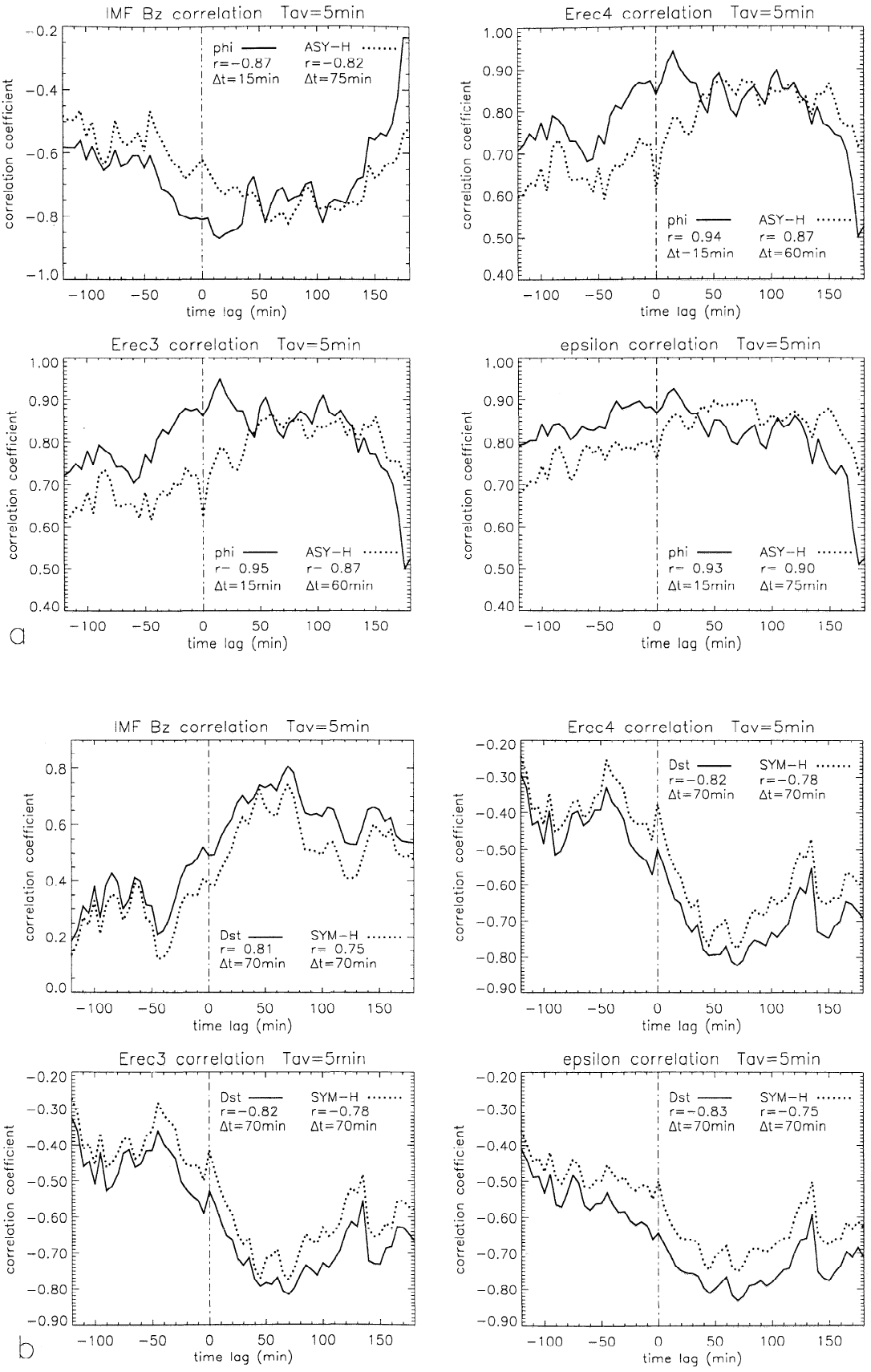

Figure 4. (a) The 5-min resolution correlation coefficient time series for Φ_{pc} and *ASY-H* with four solar wind parameters (indicated above each plot). The maximum correlation coefficient and the time lag where this occurs is shown explicitly. (b) The 5-min resolution correlation coefficient time series for *SYM-H* and *Dst*. The total time lag period ranges from -120 to 180 min.

need an improved quality measure for the correlation coefficient rather than utilizing the reduced chi-square.

3.3. Bootstrap Algorithm and the Definition of a Significance Coefficient

The bootstrap algorithm was first introduced in 1979 as a computer-based method for estimating the standard error of an empirical statistical distribution [*Efron and Tibshirani*, 1993]. An advantage of this method for assessing a statistical accuracy is that it does not rest on a normal-theory assumption.

Facing a set of 37 points between the cross-polar potential and a time-delayed solar wind parameter with an assumed linear dependence, we may calculate a correlation coefficient r. We may also view the set of 37 points with correlation coefficient r as a random sample $\mathbf{x}=(x_1,\ldots,x_{37})$ from an unknown distribution F, and we wish to estimate the accuracy of our correlation coefficient based on $\mathbf{x}$.

The general idea behind the bootstrap method is to resample $\mathbf{x}$ by randomly drawing n=37 points from $\mathbf{x}$ with replacement thus getting $\mathbf{x}^*$. The new set $\mathbf{x}^*$ consists of members of the original set $\mathbf{x}$, where some points appear more than once, and others not at all. Corresponding to $\mathbf{x}^*$, we may calculate a new correlation coefficient r^*. By independently drawing a very large number B of new sets like $\mathbf{x}^*$ and computing all their corresponding correlation coefficients (the so-called bootstrap replication), we may estimate a standard error of the original r by an empirical standard deviation of the replications $\mathbf{r}^*$ as

$$\widehat{se_B} = \sqrt{\sum_{b=1}^{B} \frac{(\mathbf{r}^*(b) - \mathbf{r}^*_m)^2}{B-1}}, \tag{1a}$$

where

$$\mathbf{r}^*_m = \sum_{b=1}^{B} \frac{\mathbf{r}^*(b)}{B}. \tag{1b}$$

It is very informative to illustrate the bootstrap replication $\mathbf{r}^*$ graphically with a histogram. This is done in Figure 5 for three different sets $\mathbf{x}$, each with n=30 points and $B = 10^5$. Going from top to bottom, we have introduced increasingly more scatter in the data. The correlation coefficient for each set is indicated in the figure. The histograms in the right column show the number of counts for each correlation coefficient. When

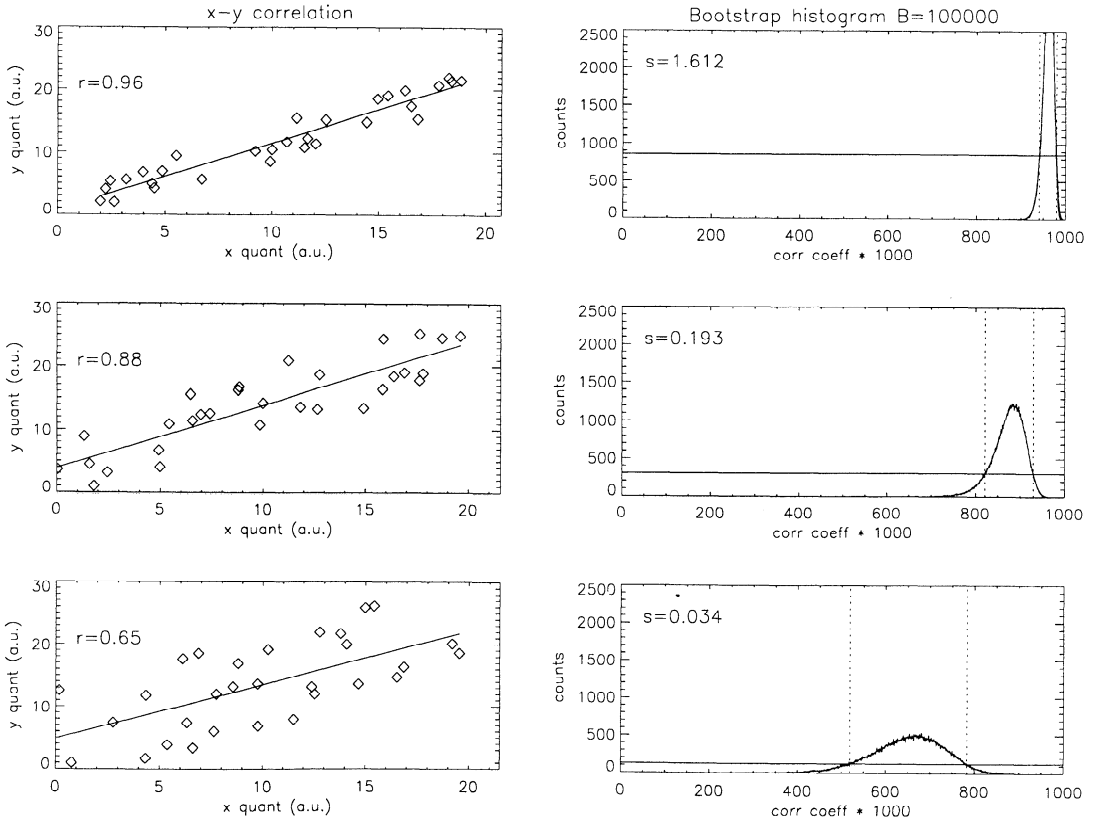

Figure 5. (left) Illustration of three examples of differently distributed data sets and (right) their corresponding bootstrap histograms where the solid horizontal line helps to mark the full width of the histogram at 25% of the peak of maximum counts. The correlation coefficient r and the computed significance parameter s (see text) are both indicated.

studying these histograms, we note that the higher the correlation coefficient is, the narrower and higher the distribution becomes, as well as getting clearly offset toward the right. We therefore define the following significance coefficient s (as already indicated in Figure 5) to help us in answering some of the questions stated earlier on the qualitative differences between correlation coefficients and we quantify this difference by,

$$s = \frac{p}{B}\sqrt{\frac{b}{fwhm \cdot \widehat{se_B}}}, \tag{2}$$

where

p maximum counts at peak of histogram;
B number of bootstrap iterations (here 10^5);
b histogram range (here 1000);
$fwhm$ full width of histogram at 25% of p.

The first factor is proportional to the peak hight of the smoothed histogram, that is, the higher the peak is the larger the significance parameter becomes. The full width at 25% of the peak histogram value, defined here as $fwhm$, and the bootstrap estimate of standard error $\widehat{se_B}$, both decrease as the correlation coefficient increases. Multiplication by the ratio $b/fwhm$ and by the inverse of $\widehat{se_B}$ thus leads to the desired effect that the significance coefficient should increase with the correlation coefficient. The square root is employed to make the significance coefficient more robust.

Two extreme situations may occur. Either the data are all aligned, in which case the histogram becomes a Dirac pulse at r=1.0, or the data are randomly distributed. As a result of the former situation, the factor p/B approaches 1.0 while both the $fwhm$ and $\widehat{se_B}$ goes to zero and the significance goes to infinity. In the latter case of a purely random distribution, the significance coefficient approaches a lower limit close to zero.

When we apply the outlined bootstrap method and the significance measure for each histogram on the correlation coefficient time series between all four magnetospheric parameters and the 5-min resolution solar wind data (see Figure 4), we get a data set of significance coefficients. By plotting the absolute value of all the correlation coefficients to their correspondingly calculated significance coefficients (see Figure 6), we observe some scatter in the significance measure which most probably originate from a combination of the computation of $fwhm$ and $\widehat{se_B}$.

To ensure a one-to-one relationship between the correlation and the significance coefficients, we fit two functions to the data. The first function, $y(x) = a\tan(x+c)$, is fitted to data where r <0.90, and the second function,

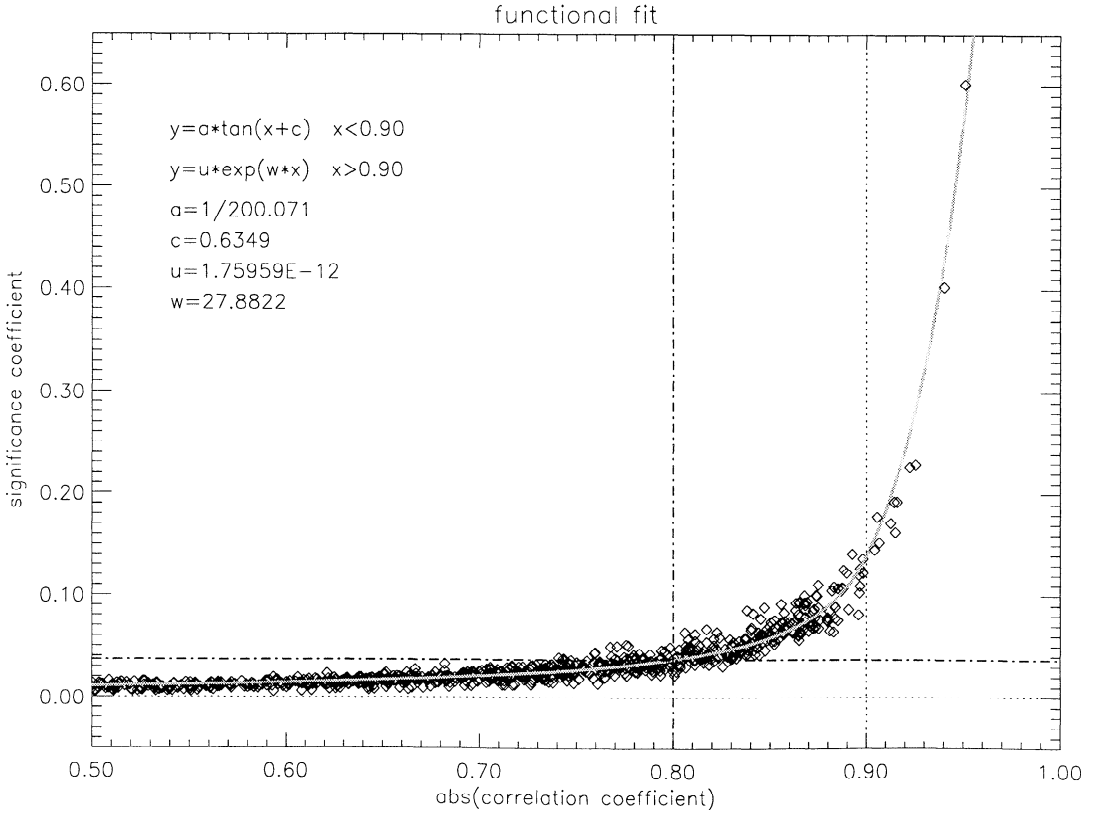

Figure 6. The functional fit of the absolute value of all correlation coefficients versus the correspondingly computed significance coefficients. Two functions are used to fit the data. These are indicated along with the derived constants.

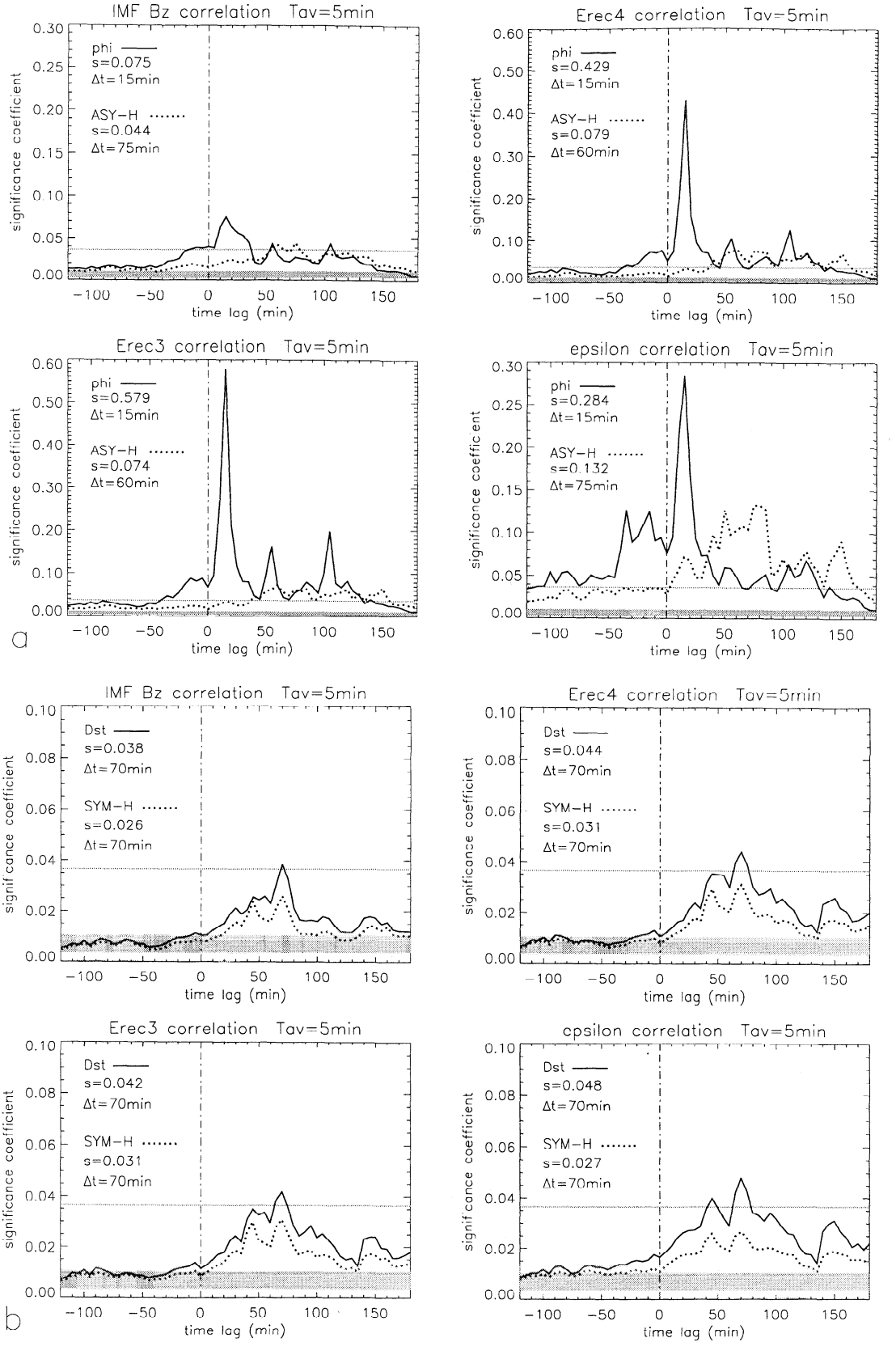

Figure 7. (a) The 5-min resolution significance coefficent time series for Φ_{pc} (solid) and *ASY-H* (dotted) where each of the coefficients are calculated using the derived functional fit (see Figure 6). Note the different scaling on the y axis. (b) As in Figure 7a for *Dst* and *SYM-H*. The maximum significance s and the time lag Δt where this occurs are shown explicitly. A grey solid horizontal line marks the significance level for a correlation coefficient of r=0.80. The grey bar along the bottom of each plot illustrates the total range of 1000 randomly distributed data sets.

$y(x) = u\exp(wx)$, is fitted to data where $r > 0.90$. The constants a and c are found by minimizing the vertical difference between each data point and $y(x)$ for $r < 0.90$, whereas the two constants u and w are found by the requirement that the two functions must have the same value of $y(x)$ as well as the same value of the derivative at $r=0.90$.

3.4. Magnetospheric Response

We are now able to substitute each correlation coefficient from the correlation time series for Φ_{pc} and *ASY-H* (see Figure 4a) into the analytical expression derived above for the significance coefficient. The resulting significance coefficient time series which is presented in Figure 7a is essentially a filtered correlation time series where different weights have been assigned objectively to each correlation coefficient depending on the shape of its bootstrap histogram. The grey bar along the bottom of each plot shows the resulting range of significance coefficients for 1000 sets of 37 randomly distributed data points using the derived analytical expression for s. A grey horizontal line marks the significance coefficient for $r=0.80$.

We observe several interesting features in the resulting significance coefficient time series for Φ_{pc} and *ASY-H*. First of all, there is a major peak at 15-min time lag in the coupling between Φ_{pc} and all solar wind parameters, a peak which is absent in the *ASY-H* response. Second, there are two additional peaks present at longer time delays in the magnetospheric response between Φ_{pc} and the reconnection electric fields. These peaks are centered at 55-min and 105-min delays, respectively, both of which are less discernible in the Φ_{pc} significance time series for ϵ. Before we proceed with a possible interpretation of the magnetospheric response as quantified by the significance parameter, we will examine some of the data behind these correlations.

The data which resulted in the peak for Φ_{pc} at 15-min time lag is shown in Figure 8 for all four solar wind parameters. The solid line in each of the four plots is the best linear least squares fit to the data using a single value decomposition technique. The intercept of this line with the y axis ranges approximately from 20 kV for Erec3 to 34 kV for ϵ.

The data resulting in the maximum correlation coefficients for *ASY-H* at 60-min and 75-min time lag are shown in Figure 9. *ASY-H* does not reduce to zero either when the solar wind parameters do. The intercepts range in this case from approximately 9 to 14 nT. Both observations of nonzero y axis interception support the existence of other mechanisms than merging.

In Figure 2 we noticed that there is some degree of correlation between Φ_{pc} and the geomagnetic indices

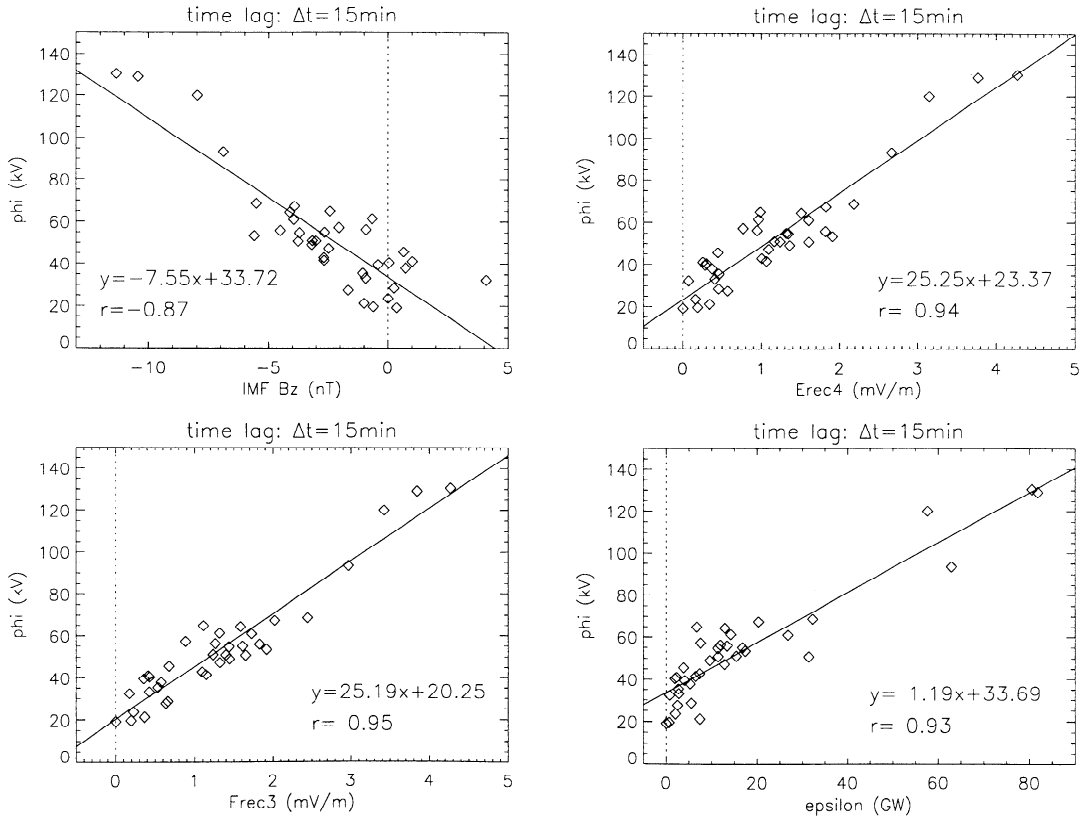

Figure 8. The contributing data for the maximum correlation between Φ_{pc} and the four solar wind parameters at a time lag of 15 min. The best fit and the corresponding correlation coefficient are both shown explicitly.

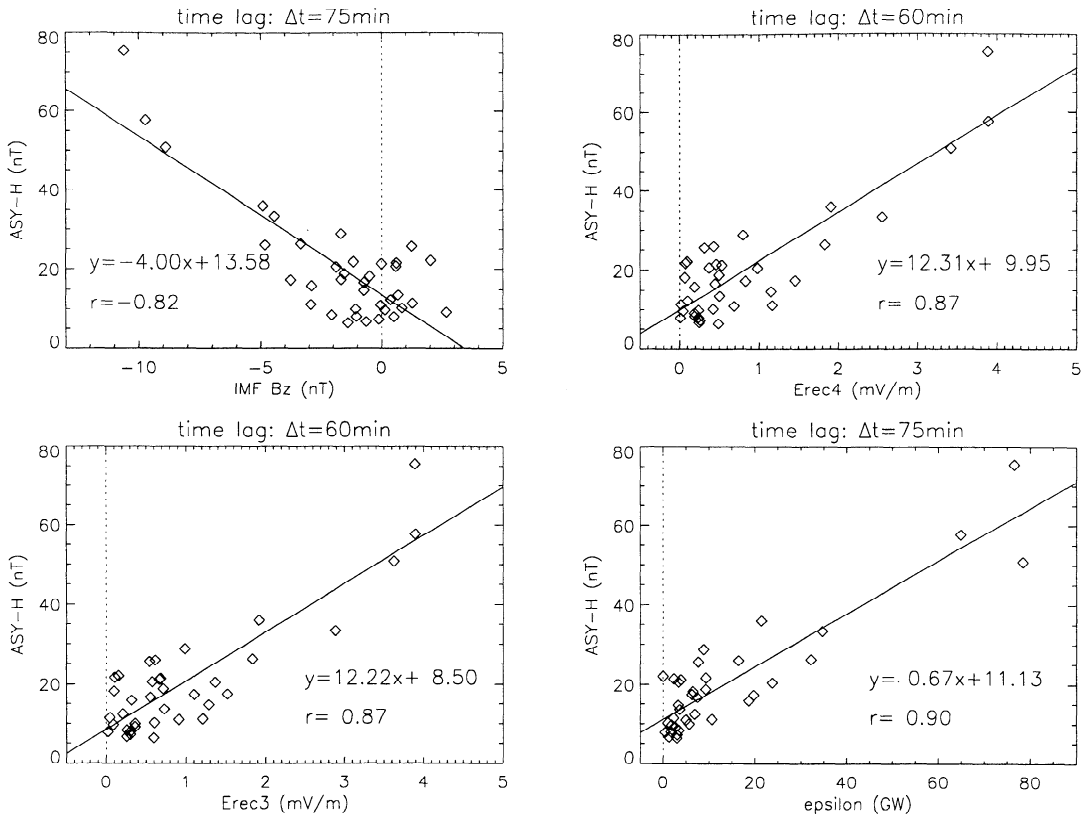

Figure 9. The data contributing to the maximum *ASY-H* correlation coefficient for IMF B_z and ϵ at 75-min time lag as well as for both models of the reconnection electric field at 60-min time lag.

Dst and *SYM-H*. The minimum *Dst* that was recorded in July 1997, which also coincided with one of the polar cap passes, reached -44 nT, while the *SYM-H* corresponding to an interval of Φ_{pc} at this time averaged to -35 nT. This is the only clear indication of any larger geomagnetic perturbation during this period which, as measured by the *Dst* index, may be classified as a small geomagnetic storm or as a typical substorm [*Gonzalez et al.*, 1994].

The corresponding significance coefficient time series for *Dst* and *SYM-H* from the correlation coefficients in Figure 4b are shown in Figure 7b. Note the different scaling on the y axis as compared with those in Figure 7a. It is clear that neither *Dst* nor *SYM-H* respond as clearly to the solar wind input as Φ_{pc} or *ASY-H* do for this particular data set. Even though the significance levels are much lower for *Dst* and *SYM-H*, we note that both indices do respond to the solar wind and that the delay is maximized at 70 min. There is furthermore evidence of a second peak at 45-min delay in the response for *SYM-H* prior to this peak. This secondary peak seems to be present as well in the correlation between *Dst* and ϵ.

We observe that while the clear direct response at 15-min time lag for Φ_{pc} is absent for all geomagnetic indices, the secondary peak at 55-min time lag between Φ_{pc} and both models of the reconnection electric field is very close to a maximum significance peak at 60-min time lag for *ASY-H*. The third peak at 105-min time lag does not seem to correspond to a similar feature in the geomagnetic data set despite its somewhat higher significance coefficient. In turning to the response with the Akasofu-Perreault ϵ parameter, we notice that the maximum response for *ASY-H* sets in at Δt= 50-85 min delay, an interval, however, where a corresponding response between Φ_{pc} and ϵ is much weaker.

4. Discussion and Conclusions

How certain are the time delays reported in the time series of the significance coefficient above? We acknowledge the fact that no account has been taken for the propagation time delay due to the subsonic plasma flow in the magnetosheath. If we assume an average bow shock location at 14 R_E, an average magnetopause location at 11 R_E and a solar wind speed of 500 km/s together with an average subsonic plasma flow between the bow shock and the magnetospause of 100 km/s, we estimate the uncertainty in the propagation time to be approximately 2.5 min since the maximum observed average solar wind speed is 494 km/s. This implies that the time delay of all significance coefficients could be

overestimated mostly by 2.5 min due to delays in the magnetosheath alone.

Clauer et al. [1983] were able to evaluate the response of the magnetosphere by investigating the relationship between vB_s and the *ASYM* index. The impulse response function for these parameters, explicitly reported by *Rostoker et al.* [1987], was found to take the general form of a Rayleigh function,

$$f(t) \sim \frac{t}{t_0} \exp^{-(\frac{t}{t_0})^2}, \quad (3)$$

where t_0 ~60 min for average levels of magnetospheric activity. This function peaks at ~40 min and returns to zero after ~120 min. In comparing the magnetospheric impulse response function $f(t)$ with the geomagnetic significance coefficient time series (see Figure 7), we observe a close resemblance with the asymmetric response of the *ASY-H* index in its correlation with the ϵ parameter. By fitting the function,

$$g(t) = c\frac{t}{t_0} \exp^{-(\frac{t}{t_0})^2} + b, \quad (4)$$

to the significance coefficients, we find a best fit for t_0 ~100 min where b and c are constants found by minimizing the difference between the function and the data (see Figure 10). A change of t_0 from ~60 to ~100 min leads primarily to a shift of the peak time response from ~40 to ~70 min and a slower decay rate which may reflect the fact that the maximum geomagnetic activity during this period is $K_p = 4^-$, that is, a moderate to low activity.

On the basis of the general agreement between $g(t)$ and the asymmetric response, we conclude that the significance coefficient time series results very well may be interpreted in terms of an average magnetospheric response to the solar wind for mostly southward IMF conditions despite the rather low statistical coverage of 37 polar cap passes with the FAST satellite.

In a recent linear prediction filter study for an ensemble of 117 isolated substorms, *Blanchard and McPherron* [1995] demonstrate that the *AL* index has two distinct modes of response to the solar wind dawn-dusk electric field vB_s. The average time lag for the two distributions was found to be 18 and 60 min. These delays include the solar wind propagation from an average bow shock at 15 R_E through the magnetosheath. They identify these modes with the *DP* 2 and the *DP* 1 current systems, respectively, and interpret the origin of these modes with dayside merging and reconnection in the magnetotail during substorms. In comparing their Figure 4 with the magnetospheric response to the ϵ parameter for Φ_{pc} and *ASY-H* (see Figure 7a), we observe a striking agreement and suggest that the peak at 15-min

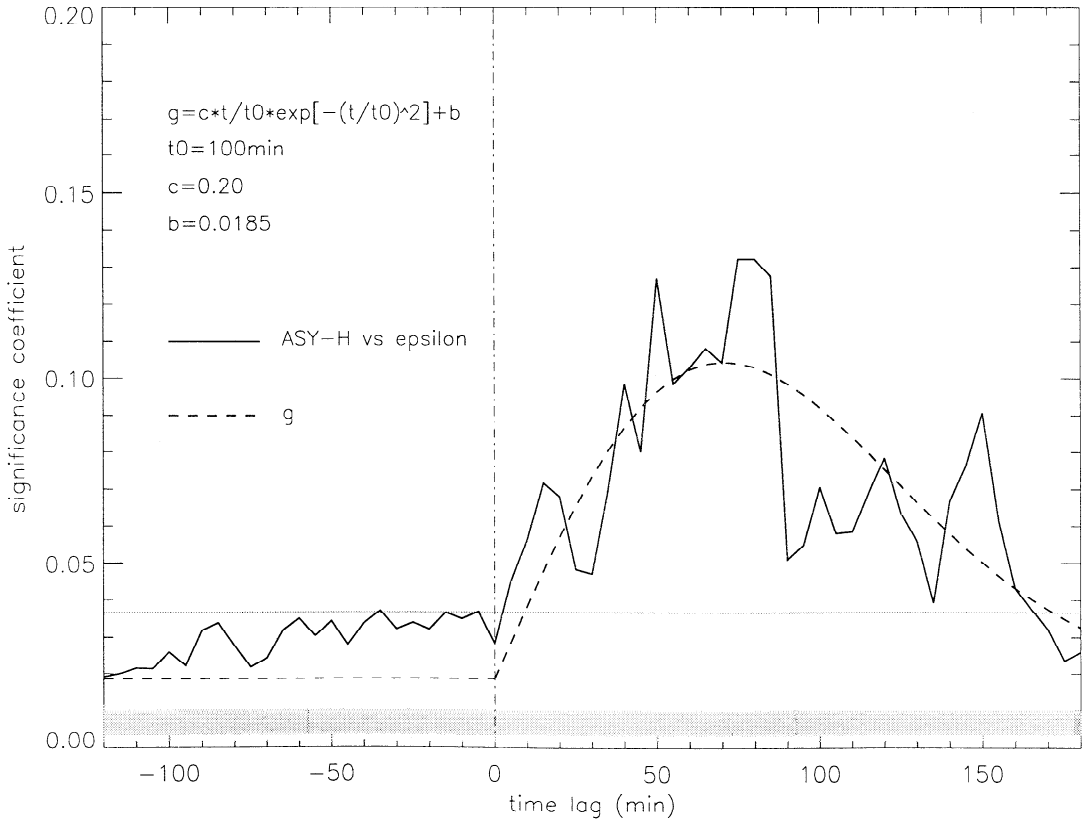

Figure 10. The best fit of the magnetospheric response function (dashed) to the significance coefficient time series between *ASY-H* and ϵ (solid).

time lag for Φ_{pc} is the directly driven average magnetospheric response of the ionospheric convection to the solar wind forcing. This response corresponds with the near 20-min pulse found by *Bargatze et al.* [1985] and is in further agreement with results reported by *Reid and Holzer* [1975] on the time constant for the ionospheric convection to adjust itself to a change in the dayside reconnection rate.

A characteristic timescale reported by *Rostoker et al.* [1987] concerns the inductive storage of energy in the Birkeland current system and their magnetospheric closure currents including the partial ring current system. This timescale was estimated by *Rostoker and Boström* [1976] to be roughly 50 min. The asymmetric significance response between *ASY-H* and ϵ at Δt= 50-85 min delay agrees very well with this timescale and with the second response mode reported by *Blanchard and McPherron* [1995]. Thus we suggest that this delay and the second peak in the cross-polar potential significance response to the solar wind electric field at 55 min is the first response of magnetotail merging with the IMF which affects both the *DP* 1 current system and the ionospheric convection.

After a further delay of 50 min, we observe a third distinct peak in the magnetospheric response between Φ_{pc} and $vB_t\sin^3(\theta/2)$ at 105 min time lag, that is, 30 min after the maximum response is seen in the correlation between *ASY-H* and the ϵ parameter. An average recurrence frequency of ~50 min was reported between substorms by *Farrugia et al.* [1993] for a 20-hour period of steady southward IMF. This recurrence period was also modeled by *Klimas et al.* [1994]. *Blanchard and McPherron* [1995] concluded that the *DP* 1 current system is driven by nightside reconnection. They further suggest that the reconnection rate in the tail depends on the solar wind electric field. Based on these results, we interpret the third peak in the cross-polar convection (see Figure 7a) response to the reconnection electric field as a second response of ionospheric convection to merging in the magnetotail, due in part to the capacitive energy stored in the global drift motion of the plasma [*Rostoker et al.*, 1987].

We recall that a high correlation of r=0.81 was found between Φ_{pc} and *ASY-H*. The proximity of the two unloading responses in the cross-polar convection with the partial ring current response between 50 and 85 min time lag is thus suggestive of a close coupling between the cross-polar convection and the system of field-aligned currents and the partial ring current as indicated by *ASY-H*.

As was further reported by *Farrugia et al.* [1993], the recurrence frequence of substorms appeared to be insensitive to the strength of the interplanetary energy input as measured by the Akasofu-Perreault ϵ parameter. This is in agreement with the absence of corresponding peak responses at 55 and 105 min time lag, respectively, in the significance coefficient time series between Φ_{pc} and ϵ (see Figure 7a).

Based on the statistical significance coefficient approach of the coupling of the solar wind with the magnetosphere, and the agreements found with earlier linear prediction studies [*Clauer et al.*, 1983; *Bargatze et al.*, 1985; *Blanchard and McPherron*, 1995], we conclude that the average response of the cross-polar convection to the solar wind electric field under southward IMF conditions at all times incorporates both the directly driven response and delayed responses due to recurrent magnetotail merging. It appears furthermore as if the cross-polar potential drop and the mid-latitude asymmetric disturbance in the H component couple to one another, though further work is needed to verify this relationship.

Acknowledgments. The first author would like to thank G. Marklund and T. Phan for valuable discussions.

Michel Blanc thanks both referees for their assistance in evaluating this paper.

References

Akasofu, S.-I., The solar wind-magnetosphere energy coupling and magnetospheric disturbances, *Planet. Space Sci., 28,* 495-509, 1980.

Baker, D. N., Statistical analyses in the study of solar wind-magnetosphere coupling, in *Solar Wind-Magnetosphere Coupling,* edited by Y. Kamide and J. A. Slavin, pp. 17-38, Terra Sci., Tokyo, 1986.

Baker, D. N., R. D. Belian, P. R. Higbie, and E. W. Hones Jr., High-energy magnetospheric protons and their dependence on geomagnetic and interplanetary conditions, *J. Geophys. Res., 84,* 7138-7154, 1979.

Bargatze, L. F., D. N. Baker, R. L. McPherron, E. W. Hones Jr., Magnetospheric impulse response for many levels of geomagnetic activity, *J. Geophys. Res., 90,* 6387-6394, 1985.

Blanchard, G. T., and R. L. McPherron, Analysis of the linear response function relating *AL* to VB_s, *J. Geophys. Res., 100,* 19,155-19,165, 1995.

Boyle, C. B., P. H. Reiff, and M. R. Hairston, Empirical polar cap potentials, *J. Geophys. Res., 102,* 111-125, 1997.

Burton, R. K., R. L. McPherron, and C. T. Russell, An empirical relationship between interplanetary conditions and *Dst*, *J. Geophys. Res., 80,* 4204-4214, 1975.

Carlson, C. W., R. F. Pfaff, and J. G. Watzin, The Fast Auroral SnapshoT (FAST) mission, *Geophys. Res. Lett., 25,* 2013-2016, 1998.

Chen, M. W., M. Schulz, and L. R. Lyons, Simulations of phase space distributions of stormtime proton ring current, *J. Geophys. Res., 99,* 5745-5759, 1994.

Clauer, C. R., and R. L. McPherron, The relative importance of the interplanetary electric field and magnetospheric substorms on partial ring current development, *J. Geophys. Res., 85,* 6747-6759, 1980.

Clauer, C. R., R. L. McPherron, and C. Searls, Solar wind control of the low-latitude asymmetric magnetic disturbance field, *J. Geophys. Res., 88,* 2123-2130, 1983.

Efron, B., and R. J. Tibshirani, *An Introduction to the Bootstrap, Monogr. Stat. Appl. Prob.,* vol. 57, 436 pp., Chapman and Hall, New York, 1993.

Fairfield, D. H., Average and unusual locations of the Earth's magnetopause and bow shock, *J. Geophys. Res., 76,* 6700-6716, 1971.

Farrugia, C. J., M. P. Freeman, L. F. Burlaga, R. P. Lepping, and K. Takahashi, The Earth's magnetosphere under con-

tinued forcing: Substorm activity during the passage of an interplanetary magnetic cloud, *J. Geophys. Res., 98,* 7657-7671, 1993.

Gonzalez, W. D., J. A. Joselyn, Y. Kamide, H. W. Kroehl, G. Rostoker, B. T. Tsurutani, and V. M. Vasyliunas, What is a geomagnetic storm?, *J. Geophys. Res., 99,* 5771-5792, 1994.

Harel, M., R. A. Wolf, P. H. Reiff, R. W. Spiro, W. J. Burke, F. J. Rich, and M. Smiddy, Quantitative simulation of a magnetospheric substorm, 1, Model logic and overview, *J. Geophys. Res., 86,* 2217-2241, 1981.

Heppner, J. P., and N. C. Maynard, Empirical high-latitude electric field models, *J. Geophys. Res., 92,* 4467-4489, 1987.

Hones, E. W., Jr., Transient phenomena in the magnetotail and their relation to substorms, *Space Sci. Rev., 23,* 393-410, 1979.

Iyemori, T., and D. R. K. Rao, Decay of the *Dst* field of geomagnetic disturbance after substorm onset and its implication to storm-substorm relation, *Ann. Geophys., 14,* 608-618, 1996.

Kan, J. R., and L. C. Lee, Energy coupling function and the solar wind magnetospheric dynamo, *Geophys. Res. Lett., 6,* 577-580, 1979.

King, J. H., Solar wind parameters and magnetospheric coupling studies, in *Solar Wind-Magnetosphere Coupling,* edited by Y. Kamide and J. A. Slavin, pp. 163-177, Terra Sci., Tokyo, 1986.

Klimas, A. J., D. N. Baker, D. A. Roberts, D. H. Fairfield, and J. Buchner, A nonlinear dynamical analogue model of geomagnetic activity, *J. Geophys. Res., 97,* 12,253-12,266, 1992.

Klimas, A. J., D. N. Baker, D. Vassiliadis, and D. A. Roberts, Substorm recurrence during steady and variable solar wind driving: Evidence for a normal mode in the unloading dynamics of the magnetosphere, *J. Geophys. Res., 99,* 14,855-14,861, 1994.

Lyons, L. R., and M. Schulz, Access of energetic particles to storm time ring current through enhanced radial diffusion, *J. Geophys. Res., 94,* 5491-5496, 1989.

Lyons, L. R., and D. J. Williams, A source for the geomagnetic storm main phase ring current, *J. Geophys. Res., 85,* 523-530, 1980.

McPherron, R. L., The role of substorms in the generation of magnetic storms, in *Magnetic Storms, Geophys. Monogr. Ser.,* vol. 98, edited by B. T. Tsurutani, W. D. Gonzalez, Y. Kamide, and J. K. Arballo, pp. 131-147, AGU, Washington, D. C., 1997.

McPherron, R. L., C. T. Russell, and M. P. Aubry, Satellite studies of magnetospheric substorms on August 15, 1968, 9, Phenomenological model for substorms, *J. Geophys. Res., 78,* 3131-3149, 1973.

Perreault, P., and S.-I. Akasofu, A study of geomagnetic storms, *Geophys. J. R. Astron. Soc., 54,* 547-583, 1978.

Reid, G. C., and T. E. Holzer, The response of the dayside magnetosphere-ionosphere system to time-varying field line reconnection at the magnetopause, II, Erosion event of March 27, 1968, *J. Geophys. Res., 80,* 2050-2056, 1975.

Reiff, P. H., and J. G. Luhmann, Solar wind control of the polar-cap voltage, in *Solar Wind-Magnetosphere Coupling,* edited by Y. Kamide and J. A. Slavin, pp. 453-476, Terra Sci., Tokyo, 1986.

Rostoker, G., and R. Boström, A mechanism for driving the gross Birkeland current configuration in the auroral oval, *J. Geophys. Res., 81,* 235-244, 1976.

Rostoker, G., S.-I. Akasofu, W. Baumjohann, Y. Kamide, and R. L. McPherron, The roles of direct input of energy from the solar wind and unloading of stored magnetotail energy in driving magnetospheric substorms, *Space Sci. Rev., 46,* 93-111, 1987.

Shue, J.-H., and D. R. Weimer, The relationship between ionospheric convection and magnetic activity, *J. Geophys. Res., 99,* 401-415, 1994.

Wolf, R. A., M. Harel, R. W. Spiro, G.-H. Voigt, P. H. Reiff, and C.-K. Chen, Computer simulation of inner magnetospheric dynamics for the magnetic storm of July 29, 1977, *J. Geophys. Res., 87,* 5949-5962, 1982.

Wygant, J. R., R. B. Torbert, and F. S. Mozer, Comparison of S3-3 polar cap potential drops with the interplanetary magnetic field and models of magnetopause reconnection, *J. Geophys. Res., 88,* 5727-5735, 1983.

C. W. Carlson, Space Sciences Laboratory, University of California, Berkeley, CA 94720-7450. (cwc@ssl.berkeley.edu)

R. E. Ergun, Department of Astrophysical and Planetary Science, Laboratory for Atmospheric and Space Physics, University of Colorado, Box 590, Boulder, CO 80309. (ree@fast.colorado.edu)

S. Eriksson, Alfvén Laboratory, Royal Institute of Technology, SE-10044, Stockholm, Sweden. (eriksson@plasma.kth.se)

W. Peria, Department of Geophysics, University of Washington, Box 351650, Seattle, WA 98195-1650. (peria@geophys.washington.edu)

(Received September 21, 1999; revised January 7, 2000; accepted February 11, 2000.)